


Harmonically trapped fermions in one dimension: A finite-temperature lattice Monte Carlo studyFelipe Attanasio¹, Marc Bauer^{1,*}, Renzo Kapust¹, and Jan M. Pawłowski^{1,2}¹*Institute for Theoretical Physics, Universität Heidelberg, Philosophenweg 16, D-69120 Heidelberg, Germany*²*ExtreMe Matter Institute EMMI, GSI, Planckstrasse 1, D-64291 Darmstadt, Germany* (Received 23 October 2023; revised 2 February 2024; accepted 14 February 2024; published 5 March 2024)

We study a one-dimensional two-component Fermi gas in a harmonic trapping potential using finite-temperature lattice quantum Monte Carlo methods. We are able to compute observables in the canonical ensemble via an efficient projective approach. Results for density profiles, correlations, as well as energy-related observables are presented for systems with up to 80 particles and various temperatures. Our simulations reproduce known numerical results and compare well against available experimental data close to the ground state, while at higher temperature they are benchmarked against the exact solution of the two-particle system. This provides an indication that a standard lattice discretization is sufficient to capture the physics of the trapped system. In the special case of a spin-imbalanced gas, we find no sign problem in the studied parameter ranges, allowing access without the need of specialized methods. This includes simulations close to the ground state and at large population imbalance, where we present results for density correlations, indicating pairing at finite total momentum.

DOI: [10.1103/PhysRevA.109.033305](https://doi.org/10.1103/PhysRevA.109.033305)**I. INTRODUCTION**

Over recent years, considerable advances have been made in the realm of ultracold atoms, both theoretically and experimentally [1–4]. The unprecedented ability to experimentally tune physical properties of the system, such as the scattering length via a Feshbach resonance [5], the shape of trapping potentials, including dimensionality [6–8], and the exact number of particles in the trap [9,10], has allowed for investigations of a wide range of physical phenomena in strongly correlated systems. In particular, pairing between fermions that experience contact interactions has been a topic of great interest for over a decade [11–15]. By tuning the scattering length, the system can be brought from a Bardeen-Cooper-Schrieffer (BCS) superfluid, where pairs are weakly bound, to strongly bound bosonic dimers, forming a Bose-Einstein-Condensate (BEC), which enables experiments to probe a rich phase structure in the crossover region [4,16,17].

In contrast to BCS-like pairing, pairs at finite momentum may form in the presence of a population imbalance. This was first studied by Fulde and Ferrell [18], and Larkin and Ovchinnikov [19], and is commonly known as FFLO-type pairing.

In this work, we investigate the thermodynamic and pairing properties of a spin-1/2 fermionic system interacting via a zero-range attractive interaction within a harmonic trapping potential in one spatial dimension. We study systems with equal and unequal number of spin-up and spin-down particles, both at finite temperature and in the ground state, which we are able to connect almost continuously.

The majority of the lattice simulations of ultracold quantum gases to date were performed without an external potential and aimed to take a thermodynamic limit. They encompass studies of ground-state and finite-temperature properties in one to three spatial dimensions [20–22], and the thermodynamics of the unitary gas [23,24] in particular. Recently, the Berezinskii–Kosterlitz–Thouless transition temperature [25], as well as pseudogap effects [26], were computed in the BEC-BCS crossover regime of the two-dimensional (2D) gas.

Previous theoretical works on the ground state of the trapped system include exact-diagonalization approaches [27–30], which are usually confined to small particle numbers. Nonuniform lattice Monte Carlo methods [31,32] have been used to study systems of up to 20 particles, while coupled-cluster [33,34] and diffusion Monte Carlo [12] approaches have allowed for computations with higher particle numbers. At finite temperature, the canonical system has been studied with exact diagonalization [35], while lattice-based methods include the grand-canonical auxiliary field and canonical stochastic Green’s function [36] approaches. Theoretical searches for exotic pairing have been carried out using, among others, Monte Carlo methods [12,36–39], diagrammatic approaches [40], and exact-diagonalization methods [35].

Lattice simulations often employ periodic boundary conditions, allowing the physical system to enjoy translation invariance. The presence of an external trapping potential breaks this symmetry, making the density profile of the atomic cloud a more interesting object and bringing the theoretical setting closer to its experimental counterpart. However, simulations at low temperature can suffer from numerical issues due to large separations of scales and require a large temporal extent of the lattice, making them computationally costly. The first

*bauer_m@thphys.uni-heidelberg.de

issue is addressed by employing safe matrix multiplication methods, while the latter is mitigated by the use of a truncation technique that removes unoccupied modes from the simulation [41]. Both methods are described in Sec. II.

While quantum Monte Carlo methods have been successfully applied to study trapped systems, as stated above, they often rely on the one-dimensional nature of the problem in order to avoid a sign problem. The lattice approach used here does not suffer from a sign problem for spin-balanced systems in any dimension. This work thus aims to lay the groundwork for future studies of trapped systems via lattice approaches, in particular in two spatial dimensions.

II. MODEL AND METHODS

The continuum Hamiltonian of the system under investigation is given by

$$\hat{H} = \int dx \hat{\psi}_\sigma^\dagger(x) \left(\frac{-\nabla^2}{2m} + \frac{1}{2} m \omega^2 x^2 \right) \hat{\psi}_\sigma(x) + g \int dx \hat{n}_\uparrow(x) \hat{n}_\downarrow(x), \quad (1)$$

where $\hat{\psi}_\sigma^\dagger$ and $\hat{\psi}_\sigma$ are, respectively, the creation and annihilation operators of fermions in spin states $\sigma \in \{\uparrow, \downarrow\}$, and the particle number density operators are given by $\hat{n}_\sigma = \hat{\psi}_\sigma^\dagger \hat{\psi}_\sigma$. In the following, we always use $m = 1$, leaving the trap frequency ω and lattice coupling g_L as parameters for the lattice systems. The choice of the lattice coupling g_L has been such that the ground-state energy on the lattice agrees with the analytical computation of a 1 + 1 particle system with coupling g ; see Refs. [31,42]. The given Hamiltonian is put on a rectangular spatial lattice of size L and spacing a with $N_x = L/a$ sites and periodic boundaries. In units of the lattice spacing, the discretized Hamiltonian then reads

$$\hat{H} = \sum_{p,\sigma} \epsilon_p \hat{\psi}_{p\sigma}^\dagger \hat{\psi}_{p\sigma} + \sum_{x,\sigma} \frac{1}{2} \omega^2 x^2 \hat{n}_{x\sigma} + \sum_x g_L \hat{n}_{x\uparrow} \hat{n}_{x\downarrow}, \quad (2)$$

where $\hat{\psi}_{p\sigma}^\dagger$ and $\hat{\psi}_{p\sigma}$ are the creation and annihilation operators for fermions with momentum p . The dispersion we use is given by $\epsilon_p = p^2/2$, which is the one of free particles. For a brief discussion on the choice of dispersion relation, see Appendix A. The parameter ω has to be chosen such that the characteristic length scale of the harmonic oscillator,

$$L_T = \frac{1}{\sqrt{\omega}}, \quad (3)$$

can be resolved, i.e., $1 \ll L_T/a \ll N_x$.

The grand-canonical partition function of the system is given by

$$Z = \text{Tr}[e^{-\beta(\hat{H} - \mu_\uparrow \hat{N}_\uparrow - \mu_\downarrow \hat{N}_\downarrow)}], \quad (4)$$

where $\beta = 1/T$ is the inverse temperature, μ_σ is the chemical potential for each spin species, and \hat{N}_σ is the respective number operator. To proceed, we cast this expression into a path-integral form by employing a Trotter decomposition, discretizing the imaginary-time evolution over N_t steps of

size $\Delta t = \beta/N_t$. Then, by performing a Hubbard-Stratonovich (HS) transformation, we rewrite the partition function of our fermionic system in the form of a path integral over a bosonic field ϕ ,

$$Z = \int \mathcal{D}\phi \det M_\uparrow(\mu_\uparrow, \phi) \det M_\downarrow(\mu_\downarrow, \phi) p(\phi), \quad (5)$$

where $p(\phi)$ accounts for the weight that depends solely on the bosonic field. The fermionic matrix is given by $M_\sigma = \mathbb{1} + U_\sigma(\mu_\sigma, \phi)$, where $U_\sigma(\mu_\sigma, \phi)$ are $N_x \times N_x$ matrices containing the information related to the kinetic energy, harmonic trap, and interaction [43,44]. In general, we may choose the fields ϕ as discrete or continuous, as well as bounded or unbounded.

A. Sampling approach

We have chosen the HS field to take values ± 1 on every lattice site, leading the path integral in (5) to become a sum over a discrete set of configurations, which we sample via the *Metropolis* algorithm. Explicitly, on each space-time point, we employ the well-known density channel transformation [45],

$$e^{-\Delta t g \hat{n}_\uparrow \hat{n}_\downarrow} = \frac{1}{2} \sum_{x_i = \pm 1} e^{(\gamma x_i - \Delta t g/2)(\hat{n}_{i\uparrow} + \hat{n}_{i\downarrow} - 1)}, \quad (6)$$

where the coupling is given by $\cosh(\gamma) = e^{-\Delta t g/2}$.

The matrix $U_\sigma(\mu_\sigma, \phi)$ is constructed using Fourier acceleration, i.e., we apply the kinetic energy in momentum space and the harmonic trap and interaction part in position space,

$$B_n(\mu, \phi) = e^{-\Delta t K} e^{-\Delta t V(\phi_n)},$$

$$U_\sigma(\mu_\sigma, \phi) = \prod_{n=0}^{N_t-1} B_n(\mu_\sigma, \phi). \quad (7)$$

In the definitions above, the chemical potential contribution can be included in either the kinetic or potential part at each step. It is not necessary to make the matrix product symmetric here, as the determinant and relevant observables all obey a form of cyclic invariance.

In practice, the costliest part of a simulation lies in constructing the matrices $U_\sigma(\mu_\sigma, \phi)$ and determinants $\det M_\sigma(\mu_\sigma, \phi)$. Naïvely, the computational cost scales as $\mathcal{O}(N_t N_x^2 \ln N_x)$ and $\mathcal{O}(N_x^3)$, respectively, which can become prohibitive for large systems or when measuring higher-order moments of observables.

At low temperatures, the matrices $U_\sigma(\mu_\sigma, \phi)$ can become ill conditioned, particularly when the relative difference between the largest eigenvalues and those around unity (indicating the Fermi surface) cannot be resolved by double precision numbers. To address this, we construct the matrices $U_\sigma(\mu_\sigma, \phi)$ using stable matrix multiplication techniques relying on intermediate QR decompositions, which have proven to be both reliable and fast [46,47].

In our simulations, we also exploit the low-rank nature of the determinant as introduced in [41]. Unoccupied modes are excluded from the simulation dynamically, resulting in matrices U_σ of size $N_x \times n_\sigma$, where n_σ is comparable to the number of particles of spin σ at low temperatures. Typically, n_σ is much smaller than N_x , leading to considerably faster computations. More precisely, the aforementioned cost

of $\mathcal{O}(N_t N_x^2 \log N_x)$ is reduced to $\mathcal{O}(N_t N_x n_\sigma \log N_x)$ for the bulk of the computation, while the determinant is computed with $\mathcal{O}(n_\sigma^3)$ operations. It is worth noting that the first QR decomposition performed when constructing U_σ remains an $\mathcal{O}(N_x^3)$ operation, which is gradually reduced to $\mathcal{O}(n_\sigma^2 N_x)$ as modes are removed. The truncation procedure is especially convenient in harmonically trapped systems, as the occupation has to be small in comparison to the system size in order to resolve the trapping potential.

Configurations are proposed via a force bias [21], resulting in acceptance rates well beyond 90%. Since a single proposal updates all fields on a single time slice, configurations are usually decorrelated within only a few sweeps of the whole lattice.

B. Reweighting to the canonical ensemble

All sampling is performed in the grand-canonical ensemble. To obtain observables in the canonical ensemble, we employ a reweighting procedure using Fourier projection [48]. The canonical partition function is given by

$$Z_N = \text{Tr}[\hat{P}_{N_\uparrow} \hat{P}_{N_\downarrow} e^{-\beta \hat{H}}], \quad (8)$$

with the projection operator

$$\hat{P}_{N_\sigma} = \frac{1}{N_x} \sum_{j=0}^{N_x-1} \exp \left[i 2\pi j \frac{N_\sigma - \hat{N}_\sigma}{N_x} \right]. \quad (9)$$

In (8), we can introduce, to the exponential additional terms, $\beta \mu_\sigma (\hat{N}_\sigma - N_\sigma)$ to stabilize the Fourier sum numerically. For practical purposes, the chemical potential is the one we use to sample the grand-canonical system, but it has no actual influence on the canonical trace. It is tuned such that the average particle number in the grand-canonical ensemble is close to the desired one in the canonical ensemble.

In a general case, the sum over projection angles must be over the full basis set of the system. However, when a truncation is applied, it is enough to consider the truncated basis size [49]. This leads to a significant decrease in computational cost in dilute systems.

We define a modified matrix for each projection angle in the Fourier sum as $M_\sigma^l = \mathbb{1} + \exp[-i 2\pi l] U_\sigma(\mu_\sigma, \phi)$, and use $z^{lm}(\mu_\uparrow, \mu_\downarrow, \phi) = \det M_\uparrow^l(\mu_\uparrow, \phi) \det M_\downarrow^m(\mu_\downarrow, \phi)$ for the weight. A measure of the overlap between the canonical and grand-canonical partition functions is given by

$$\langle W_N \rangle = \left\langle \frac{1}{N_x^2} \sum_{l,m} e^{\frac{i(N_\uparrow + m N_\downarrow)}{2\pi N_x}} \frac{z^{lm}(\mu_\uparrow, \mu_\downarrow, \phi)}{z(\mu_\uparrow, \mu_\downarrow, \phi)} \right\rangle, \quad (10)$$

where the expectation value is with respect to the grand-canonical weight. We omit the chemical potential prefactor since it only gives a normalization, dropping out of observables. Note that the ratio does not necessarily need to be close to unity for good statistics, as the partition functions are not normalized. In practice, low ratios do not seem to pose a problem, as long as the relative fluctuations in (10) are small. This is generally the case when the average particle number of the grand-canonical system agrees with the target particle number of the canonical one. At higher temperatures, we can usually reweight to a larger range of particle numbers. The

computation of observables proceeds similarly, now including an additional sum over projection angles,

$$\langle O \rangle_N = \frac{1}{\langle W_N \rangle N_x^2} \times \left\langle \sum_{l,m} e^{\frac{i(N_\uparrow + m N_\downarrow)}{2\pi N_x}} \frac{z^{lm}(\mu_\uparrow, \mu_\downarrow, \phi)}{z(\mu_\uparrow, \mu_\downarrow, \phi)} O_N^{lm}(\phi) \right\rangle. \quad (11)$$

For the one-body density operator, the observable to be computed is

$$n_{ij,N}^{lm}(\phi) = [(\mathbb{1} + e^{i 2\pi l / N_x} U^{-1})^{-1}]_{ij}, \quad (12)$$

which is independent of the index m , since the different spin species factorize. Higher-order observables are computed using the one-body operator and Wick's theorem in analogy to the grand-canonical case. To ensure efficient computation of the canonical observables, the U matrices are diagonalized, again making use of the truncation similar to what is introduced in [49]. This works by taking advantage of the reduced matrix sizes at low particle numbers, extracting only the relevant eigenvalues and eigenvectors.

In a general situation, for instance at positive coupling g or in the presence of spin imbalance, positivity of the weight is not guaranteed. This is accounted for in our simulation by standard reweighting. In practice, we always sample the absolute value of the grand-canonical weight and perform the full reweighting in a single step with the projection to the canonical ensemble.

C. Ground-state projection

The finite-temperature simulations described above are well suited for the simulations of the system at temperatures close to $T = 0$. However, they are not designed for the explicit computation of the ground state, Ψ_0 . To address this, we complement the finite-temperature simulations with a ground-state projection in the canonical ensemble, following the method described in detail in, e.g., [46,50]. This projective method relies on a trial state Ψ_T , which is taken to be a Slater determinant, and uses that for nonvanishing overlap $\langle \Psi_T | \Psi_0 \rangle \neq 0$, the trial state converges to the ground state,

$$\lim_{\beta \rightarrow \infty} e^{-\beta \hat{H}} |\Psi_T\rangle = |\Psi_0\rangle. \quad (13)$$

We choose the trial state as the exact solution of the non-interacting system, although more sophisticated options are possible. For the ground-state projection, the imaginary-time evolution is split into N_t steps of size $\Delta t = \beta / N_t$. At each time slice, we apply a symmetric Trotter decomposition and utilize Fourier acceleration when applying them to the states. Again, we make use of QR decompositions to allow for a stable evolution of the Slater determinants. Moreover, to handle the Hamiltonian's interaction term, we use the same HS transformation as for the finite-temperature simulation from (6). The respective auxiliary fields are again sampled using the force bias method. Altogether, this leads to a ground-state projection operator of the form

$$e^{-\beta \hat{H}} \approx \prod_{n=1}^{N_t} e^{-\Delta t K/2} e^{-\Delta t V(\phi_n)} e^{-\Delta t K/2}. \quad (14)$$

The observables O are then computed using the symmetric estimator,

$$\langle O \rangle_{\text{GSP}} = \frac{\langle \Psi_T | e^{-\beta \hat{H}/2} O e^{-\beta \hat{H}/2} | \Psi_T \rangle}{\langle \Psi_T | e^{-\beta \hat{H}/2} e^{-\beta \hat{H}/2} | \Psi_T \rangle}. \quad (15)$$

This concludes our setup.

III. RESULTS

Our results are structured as follows. In Sec. III A, we provide a brief discussion on the lattice size and parameters. Section III B presents results for density profiles and correlations in systems with balanced population. In Sec. III C, we provide a comparison to exact-diagonalization results for separation energies and compute the temperature dependence of the pairing gap for various particle numbers. Finally, in Sec. III D, we briefly discuss the sign problem and provide a tomographic picture of density-density correlations in the imbalanced system.

A. Lattice parameters

An essential aspect of lattice simulations is the choice of parameters to ensure a rapid convergence towards the continuum limit. In our case, there are several limits that need consideration. One is the temporal lattice spacing a_τ , which dictates the number of time slices used and thus influences the error of the Trotter decomposition. In all situations studied here, we find $a_\tau/a = 0.05$ to be sufficiently small to ensure a negligible Trotter error.

The ratio L_t/a governs the finite-size and finite-distance errors and is set to $L_t/a = 4$. Simultaneously, the total number of spatial sites is $N_x = 80$, which corresponds to a box size of $N_x/L_t = 20$ in units of the harmonic oscillator. We find these parameters to be sufficient for the system with up to $N = 20$ particles studied in the main text, which corresponds to a total filling of $N/N_x = 0.25$. However, it is worth noting that a higher number of particles necessitates both a larger spatial extent and smaller spacing, in order to avoid finite-size and filling effects. In particular, one must ensure that the center of the trap is sufficiently below the saturation density, which is the case in all our computations. In Appendix B, we consider systems with up to $N = 80$ particles, for which we use a $N_x = 200$ lattice and $L_t/a = 8$, leading to $N_x/L_t = 25$ and a filling of $N/N_x = 0.4$. The proximity to the continuum theory is evidenced by the excellent agreement with previous results found, e.g., in Figs. 3 and 6. Additionally, we have compared the density profiles for $N = 20$ fermions for various lattice parameters and find them to fall on universal curves; see Appendix C.

For the system with $1 + 1$ particles, the continuum Hamiltonian can be diagonalized analytically, yielding an exact comparison for observables in the canonical ensemble. To determine the appropriate bare lattice coupling, we tune it such that it yields the exact ground-state energy of the two-particle system, given by the relation for the continuum coupling [42,51],

$$g(E) = \frac{\sqrt{2}(E-1)\Gamma(1-\frac{E}{2})}{\Gamma(\frac{3}{2}-\frac{E}{2})}. \quad (16)$$

Achieving this does not require a direct lattice simulation, as the two-particle lattice system can be numerically diagonalized, providing the desired ground-state energy.

B. Spin-balanced gas

In the case of spin-balanced systems, the determinants in (5) are real and equal, since $\mu = \mu_\uparrow = \mu_\downarrow$ and thus no sign problem is present. This is true for the density channel Hubbard-Stratonovich transformation used in this work, as well as the spin- z channel not applied here, where the determinants are complex conjugate of each other.

Before making further use of the particle number projection methods described above, we computed the expectation value of the particle number operator $\hat{N}_\sigma = \int dx \hat{n}_\sigma(x)$ as a function of the chemical potential for different temperatures, along with the correlation between up and down spin number operators, $\langle \hat{N}_\uparrow \hat{N}_\downarrow \rangle - \langle \hat{N}_\uparrow \rangle \langle \hat{N}_\downarrow \rangle$.

Figure 1(a) depicts clear steps at nearly integer particle numbers for the lowest temperature of $T/\omega = 0.125$, indicating the thresholds in chemical potential where each energy level is filled. This effect is smoothed by thermal fluctuations, as can also be seen. Moreover, the attractive interaction between up and down spins causes the departure from the empty system to occur at negative chemical potentials. The noninteracting theory, on the other hand, would have this threshold around $\mu/\omega = 1$ for small but finite temperature.

Figure 1(b) shows the (connected) correlation between \hat{N}_\uparrow and \hat{N}_\downarrow . Similar to what can be seen in the average particle number, this correlation function for $T/\omega = 0.125$ exhibits repeating behavior following the filling of the different energy levels. Conversely, at high temperature, this behavior is not present and the correlator changes more smoothly with the chemical potential.

Turning to the canonical ensemble, we investigate the density profile of a fixed number of particles in the trapping potential. The ground state shows characteristic particle peaks, originating directly from the wave functions of the harmonic-oscillator states. These oscillations are already present in the ground state of the noninteracting system $g = 0$, where the density is given by $n^{(0)}(x) = \sum_{n=0}^{N_\sigma-1} |\psi_n(x)|^2$, in terms of the well-known harmonic-oscillator wave functions $\psi_n(x)$. The density peaks are thus not necessarily a sign of pairing, but rather a direct consequence of the harmonic potential.

In Fig. 2(a), the density profile $n(x) = n_\uparrow(x) = n_\downarrow(x)$ for $g/\sqrt{\omega} = -3$ with $3 + 3$ particles is plotted for various temperatures. In the ground state, the density distribution displays three peaks, equal to the number of filled oscillator shells. The same behavior is observed at temperatures significantly smaller than the spacing between energy levels in the trapping potential, where the ground-state contribution dominates. As the temperature increases to the point where the thermal energy becomes comparable to the energy gap, the peaks disappear and the density profile gradually smoothens.

With larger particle numbers, the particle peaks are expected to decrease in amplitude and become more frequent, eventually converging towards a smooth profile in the thermodynamic limit (see Appendix B).

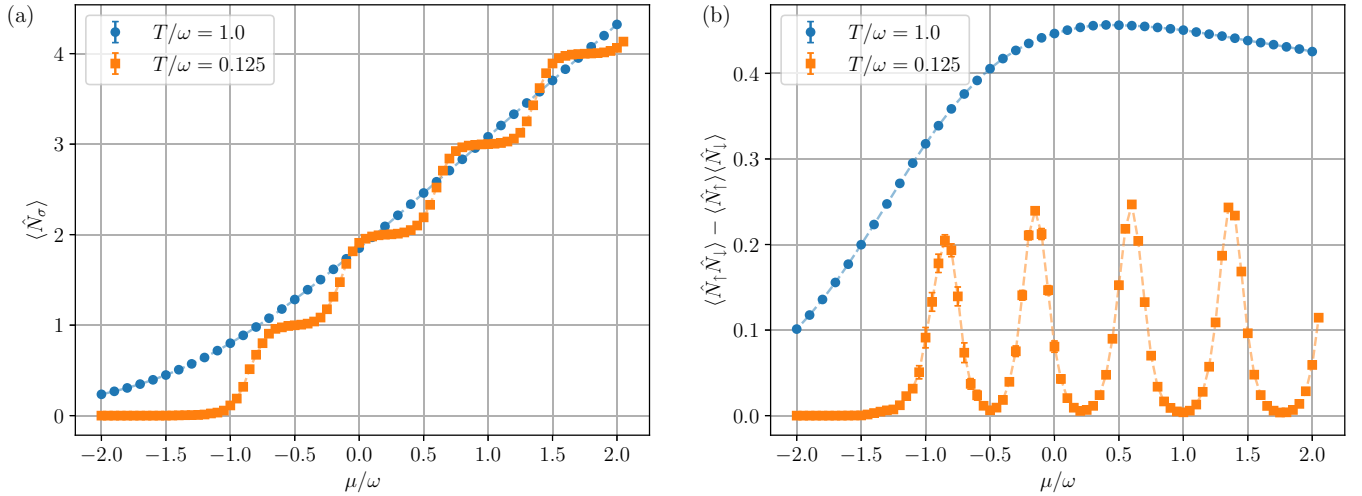


FIG. 1. (a) Expectation value of the particle number operator as a function of the chemical potential $\mu = \mu_\uparrow = \mu_\downarrow$ for different temperatures at $g/\sqrt{\omega} = -3$. (b) Correlation between the particle number operators for each spin species as a function of the chemical potential $\mu = \mu_\uparrow = \mu_\downarrow$ for different temperatures at $g/\sqrt{\omega} = -3$. Dashed lines are drawn to guide the eye.

As an indicator for the existence of pairing in the system, we compute the connected density-density correlation function in momentum space, given by

$$S(k, k') = \langle n_\uparrow(k) n_\downarrow(k') \rangle - \langle n_\uparrow(k) \rangle \langle n_\downarrow(k') \rangle. \quad (17)$$

Pairing around the Fermi surface is expected to manifest as positive correlation peaks at $S(\pm k_F, \mp k_F)$. In Fig. 2(b), we present results for the system at $g/\sqrt{\omega} = -3$ and $S(k, -k)$ for various temperatures. Close to the ground state, the peaks around the Fermi surface are more pronounced. The correlations decrease rapidly towards larger momenta, but they do not vanish at vanishing opposite momenta due to the finite particle number and the resulting finite size of the systems, as compared to the thermodynamic limit of an untrapped gas. We observe a weakening in correlations, similar to the

breakup of ground-state features in the density profile, when temperatures become comparable to the level spacing of the trapping potential. However, in contrast to the oscillations in the density profile, the density-density correlations at higher temperatures remain clearly visible. While the peaks around the Fermi surface are less pronounced, the overall correlation appears flatter at small momenta.

C. Energy observables

Having explored density observables and their correlations, we now shift our focus to energy-related quantities. In particular, separation energies have been measured experimentally [52] and studied theoretically via exact diagonalization [28,34], and provide a good benchmark for the validity of our computations close to the ground state. The separation energy can be understood as the interaction energy cost of adding a

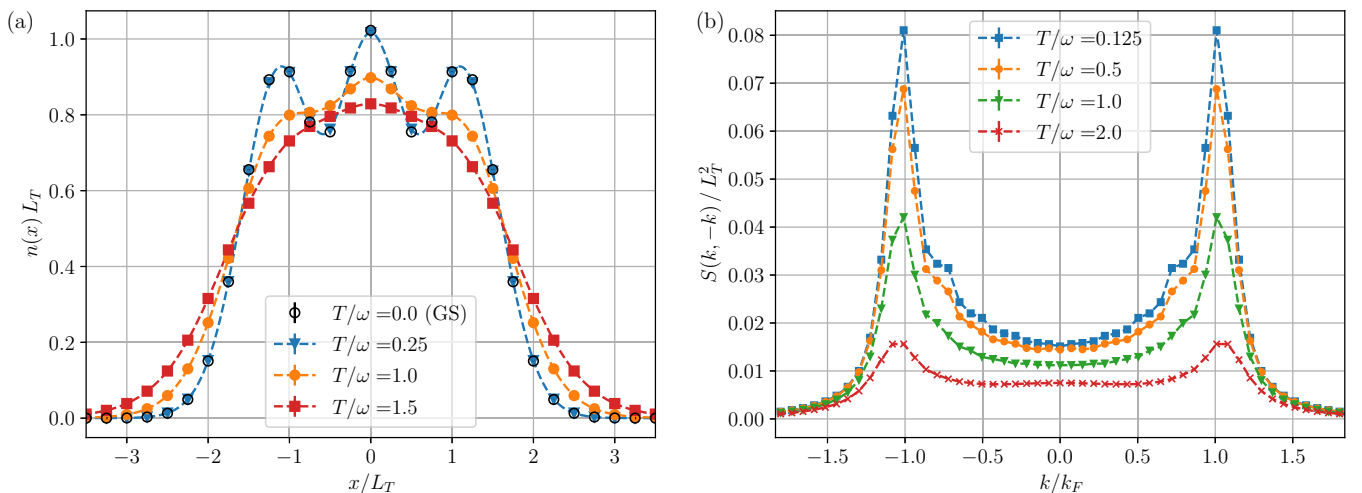


FIG. 2. (a) Density profile per spin species $n(x) = n_\uparrow(x) = n_\downarrow(x)$ for $3+3$ particles and $g/\sqrt{\omega} = -3$ at three different temperatures. Dashed lines are splines through the data points and hollow circles indicate data from projection to the ground state. (b) Antidiagonal of the density-density correlation function for $10+10$ particles at $g/\sqrt{\omega} = -3$ and four different temperatures.

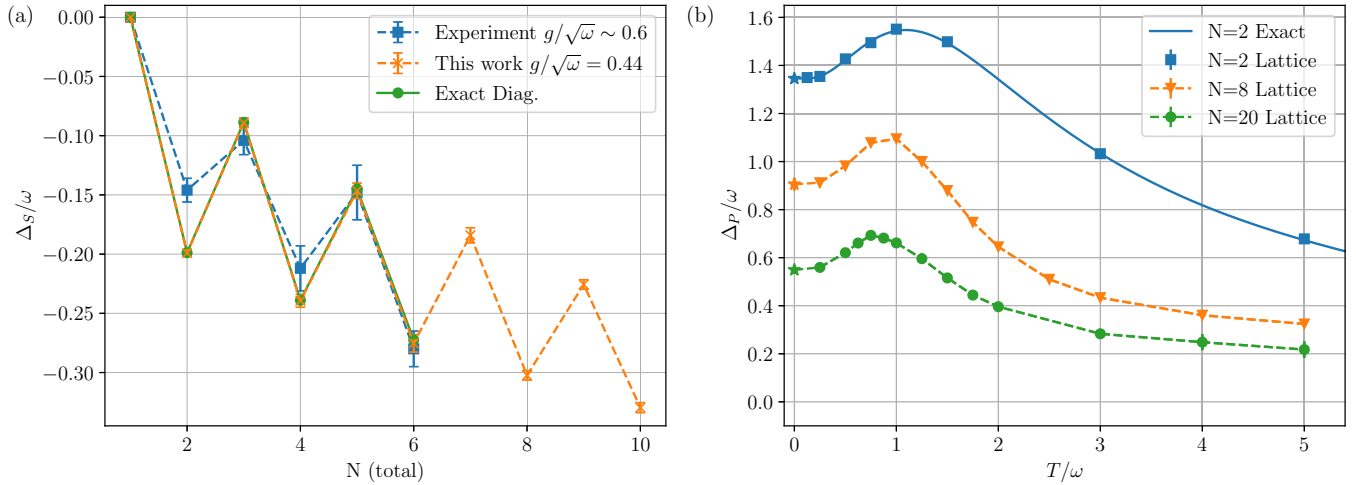


FIG. 3. (a) Separation energies in the ground state for up to 5 + 5 particles. Experimental data [52] (blue squares) and exact-diagonalization results [28] (green circles) are compared to results from finite-temperature lattice simulations at $T/\omega = 0.125$ (orange cross). (b) Pairing gap at $g/\sqrt{\omega} = -3$ for 1 + 1, 4 + 4, and 10 + 10 particles at finite temperatures. The two-particle system is compared to the exact result of the continuum theory (solid line). Stars indicate results from ground-state projection.

single particle to the system and is defined in terms of the ground-state chemical potential of the system as follows:

$$\mu(N) = E(N) - E(N - 1), \quad (18)$$

$$\Delta_S(N) = \mu(N) - \mu^*(N), \quad (19)$$

where $\mu^*(N)$ is the chemical potential of the free system.

At low temperatures, this requires simulations of an imbalanced system, since the overlap of the balanced canonical simulation with the imbalanced sector becomes small. In Fig. 3(a), we observe excellent agreement between our results, marked as “Lattice” and computed with a finite temperature of $T/\omega = 0.125$, and results computed via the exact-diagonalization method from [28]. The steplike behavior, with lower energies for even particle numbers, which correspond to shell closures, indicates the presence of pairing between particles of up and down spin. We also note the proximity to experimental values at a slightly different coupling. Some deviations are visible in comparison to the experiment, likely due to anharmonicity in the trapping potential present in the experiment, while beyond the scope of this work, our method generally allows the study of an arbitrarily shaped external potential, which opens up avenues to study the effects of anharmonicity in a controlled manner. For the comparison to exact-diagonalization results, we match both two-body energies to the same ground-state values, resulting in a value for the coupling that is slightly smaller than what was given in [28]. While the results in Fig. 3(a) are at small coupling, similar agreement with exact diagonalization is found in more strongly coupled scenarios.

Next, we compute the energy staggering pairing gap, defined for even particle numbers as

$$\Delta_P(N) = \frac{1}{2}[2E(N/2 - 1, N/2) - E(N/2, N/2) - E(N/2 - 1, N/2 - 1)]. \quad (20)$$

This quantity serves as an indicator for pairing in the system and has been used to study pseudogap effects [15,26] and pair

correlations [13] in higher dimensions. Although higher-order estimators are available [53], we use a three-point estimator here for simplicity. At high enough temperatures, it is often enough to sample for a single chemical potential and reweight the different particle numbers from the same data. This approach breaks down around $T/\omega \sim 0.5$, where we perform an independent simulation for the energies at different particle numbers.

Figure 3(b) depicts the pairing gap at $g/\sqrt{\omega} = -3$ for 1 + 1, 4 + 4, and 10 + 10 particles at finite temperature. For two particles, we find good agreement with the exact result of the continuum theory up to $T/\omega = 5$. We see an increase in the gap when increasing temperature, before it decays again. This behavior can likely be explained by the lower degeneracy in the first few excited states of the 1 + 1 system compared to its noninteracting counterpart. Consequently, the energy of the single-particle contribution increases more rapidly than that of the two-particle one. The good agreement of the two-particle systems with the exact result indicates the validity of the renormalization approach used to fix the coupling, where no excited states were considered. However, we expect the agreement to break down at higher temperatures, as high-energy states beyond the limits of the lattice start to contribute significantly.

The systems with 8 and 20 particles, respectively, follow a similar general trend to the two-particle one, but at lower total magnitude, consistent with available ground-state results [33]. Interestingly, we still find peaks at finite temperature, which move to lower temperature when increasing the particle number. It remains unclear, from our computations, whether the peak converges to a fixed temperature or vanishes in the thermodynamic limit, indicating a shell effect.

D. Imbalanced gas

An important open question in the study of ultracold fermionic gases is the existence of an exotic pairing phase at finite spin imbalance. Such a phase, known as the FFLO

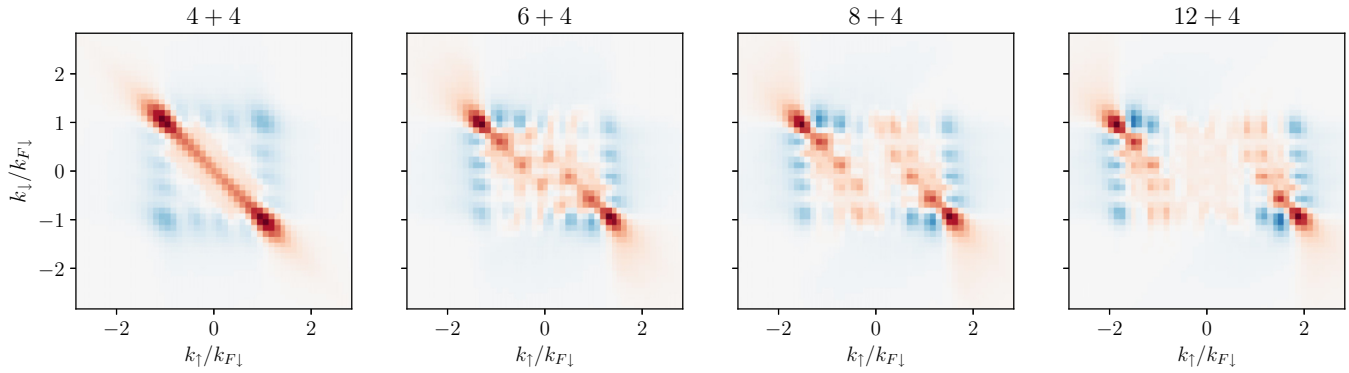


FIG. 4. Density-density correlations of the system at $g/\sqrt{\omega} = -3$ and $T/\omega = 0.25$, with varying imbalance. We observe clear signals of unconventional pairing in the presence of an imbalance. To retain visibility, all color scales are normalized independently to span the full range of values in the corresponding data.

phase, is characterized by pairing at nondegenerate Fermi surfaces, resulting in pairs with finite total momentum $k_{F\uparrow} - k_{F\downarrow}$.

It is not clear, however, to what extent such systems can be studied using standard lattice methods. In the case of imbalanced spin species, the configuration weight is not necessarily positive anymore, and a sign problem can arise. This is the case in both 2D and 3D simulations [54,55]. In contrast, some previous studies of Fermi gases with contact interactions in 1D have not shown a sign problem in the considered parameter regions [56–58]. The trapped system considered here appears to show similar behavior. For no temperature, chemical potential, or coupling that has been studied do we find negative weight configurations. It is important to note that this is not an issue of ergodicity, as our code runs into the expected sign problems in 2D and 3D and reproduces known results in 1D as has already been shown above in the case of separation energies, which require simulations at a slight imbalance.

We complement previous studies that consider trapped systems with imbalances [35,36,59] by computing pairing patterns at higher particle numbers than done previously. In Fig. 4, we present a visualization of the connected density-density correlations in (17) for a system with 4 + 4 to 4 + 12 particles at $g/\sqrt{\omega} = -3$ and $T/\omega = 0.25$ in momentum space. The spin-balanced system is peaked at $k_{\uparrow} + k_{\downarrow} = 0$, while the imbalanced systems show a clear signal of pairing at finite momentum, which is consistent with the expected FFLO behavior. It is important to note that Fig. 4 does not show the relative magnitude of correlations at different particle numbers; each plot is independently normalized to ensure visibility. Moreover, several pockets of positive and negative correlation are visible, forming an oscillatory pattern. These oscillations, similar to the oscillatory pattern in the density profile, are a feature of the harmonically trapped system, not found in the same way in the untrapped gas [37]. While a thorough analysis is left to future work, we generally find a decrease in correlations when going to higher temperatures and larger imbalance, which aligns with results from a recent exact-diagonalization study of few-particle systems at finite temperature [35].

IV. CONCLUSION

We have presented results from lattice simulations of trapped fermionic systems in one dimension, in both the case of balanced and imbalanced populations. The sampling was performed in the grand-canonical ensemble with a reweighting step to give canonical expectation values, which is more efficient than directly sampling the canonical weight but requires tuning the chemical potential. The stabilization procedure we used allowed us to simulate the full range of temperatures, down to the ground state, where we compare to a projective approach. To verify the validity of our results, we compared to experimental and theoretical data for the separation energies of up to six particles, finding good agreement. Additionally, we computed the energy staggering pairing gap, which agrees with exact results for the two-particle system and is also computed for up to 20 particles. The computation of separation energies in particular requires simulations for spin-imbalanced systems, which we find to be sign-problem free in the studied parameter ranges. This is also the case when computing density-density correlations in the presence of larger imbalances, where we find clear signals of unconventional pairing.

In future studies, it may be interesting to explore polaronic effects in the systems, as no sign problem appears to be present, allowing computations even at large imbalances. In this paper, we put a focus on attractive contact interactions due to the absence of a sign problem. However, recent work on the application of complex Langevin methods in the study of both ultracold fermions [37–39,60,61] and bosons [62–64] may allow for the study of repulsive interactions in the future. In contrast to, e.g., Path integral Monte Carlo computations, the canonical lattice formulation used in this work does not incur a sign problem in higher dimensions, as long as the population remains balanced. Given the good agreement of our lattice computation to previous results in, e.g., Fig. 3(a), we expect the approach to generalize straightforwardly to higher dimensions. Indeed, using a very similar truncation approach as the one employed here, lattices for up to 75^2 were recently studied in the two-dimensional untrapped gas [25], which is close to the linear extent that we found to be sufficient for the 1D system.

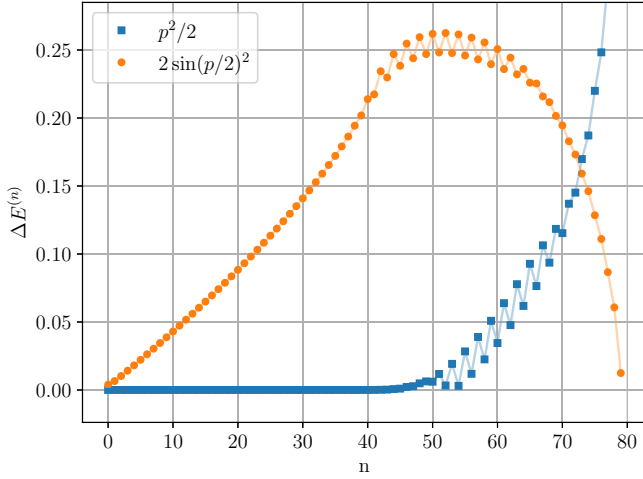


FIG. 5. Relative deviation of the energy levels with p^2 dispersion and Hubbard dispersion in the noninteracting lattice system compared to the continuum theory.

ACKNOWLEDGMENTS

We thank P. D’Amico for discussions and data. We also thank S. Shokri and M. Haverkort for discussions. This work is funded by the Deutsche Forschungsgemeinschaft (DFG, German Research Foundation) under Germany’s Excellence Strategy EXC 2181/1 - 390900948 (the Heidelberg STRUCTURES Excellence Cluster) and the Collaborative Research Centre SFB 1225 - 273811115 (ISOQUANT). We also acknowledge support by the state of Baden-Württemberg through bwHPC.

APPENDIX A: LATTICE DISPERSION

The discretization of the Laplace operator is an important aspect of lattice simulations. In particular, a well-chosen dispersion can reduce finite distance effects and improve

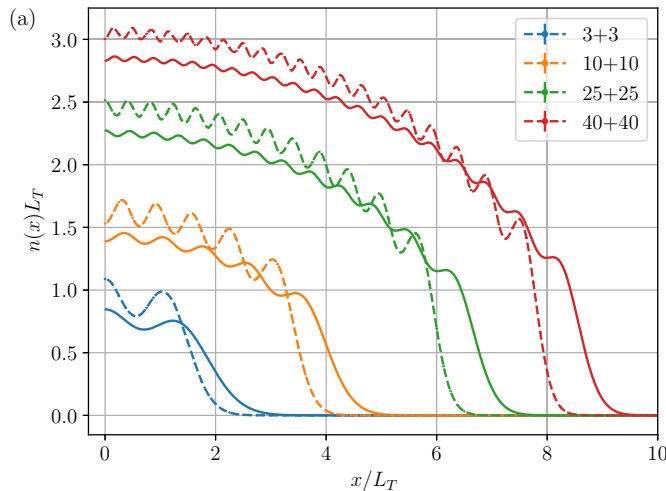


FIG. 6. (a) Density profiles per spin species for $N = 6, 20, 50,$ and 80 particles at $g/\sqrt{\omega} = -5$ and $T/\omega = 0.25$. Splines connecting the data points (dashed lines) are drawn to guide the eye. The ground-state densities of the corresponding noninteracting systems are plotted as solid lines. (b) Energy of the system, normalized by the noninteracting energy, as a function of the rescaled coupling γ . The energies of the two-particle system in the ground state are plotted as a dashed line.

convergence to the continuum limit. In this work, we use

$$\epsilon_p = \frac{p^2}{2} \quad (\text{A1})$$

for the kinetic energy of the lattice system. Another form often used is given by the finite-difference approximation of the derivatives, yielding

$$\epsilon_p = 2 \sin^2\left(\frac{p}{2}\right), \quad (\text{A2})$$

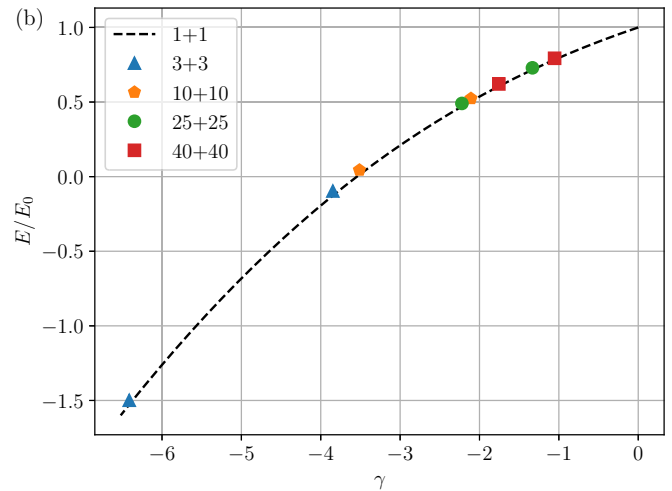
which is the standard dispersion of the Hubbard model, which was previously used for the trapped system in, e.g., [36]. As a simple check, we diagonalize the noninteracting lattice Hamiltonians with both dispersions and compare the resulting energies to the continuum theory. The lattice parameters from the main text are used, which are $N_x = 80$, $\omega = 0.0625$. In Fig. 5, we compare the energy levels of the lattice Hamiltonians to those of the continuum theory,

$$\Delta E^{(n)} = \frac{|E^{(n)} - E_{\text{cont}}^{(n)}|}{E_{\text{cont}}^{(n)}}. \quad (\text{A3})$$

The quadratic dispersion shows significantly better agreement, with no significant deviations up to half filling, while the Hubbard dispersion deviates even for the lowest-lying states. In both cases, we observe an even-odd effect in higher shells. This is not an issue for our simulations, as they are carried out in more dilute regimes. Figure 5 suggests that it is necessary to use the quadratic dispersion if one wants to obtain accurate results for observables such as the total energy or separation energies. It should be noted that methods which keep the energy levels exact are available, but require a nonuniform spatial lattice [31,32].

APPENDIX B: LARGE PARTICLE NUMBERS

To show the applicability of our approach to systems of large particle number, we compute the density profiles and



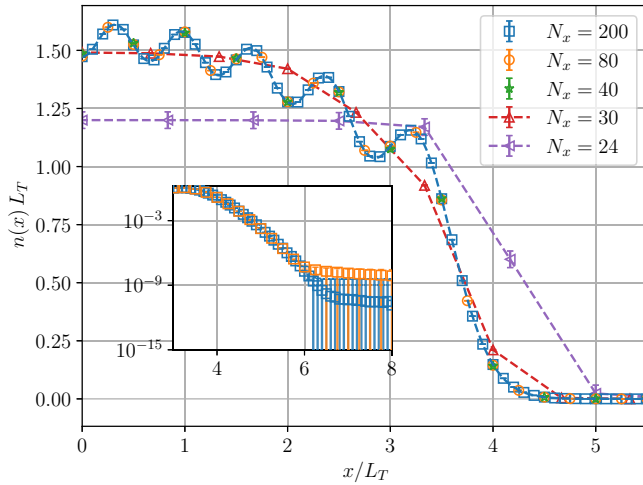


FIG. 7. Density profile for the $N = 20$ balanced system at various lattice sizes. The inset shows the tails of the density profile on a logarithmic scale.

energies for systems of up to $N = 80$ particles. To this end, we adjust the lattice parameters to be $N_x = 200$ and $\omega = 0.015625$, which corresponds to $L_T/a = 8$. In Fig. 6(a), we plot the density profiles $N = 6, 20, 50$, and 80 particles at $g/\sqrt{\omega} = -5$ and $T/\omega = 0.25$, as well as the ground-state densities of the corresponding noninteracting systems. The larger number of lattice sites, and smaller lattice spacing, allow for a satisfactory resolution of the density oscillations close to the ground state. To further verify the computations, we compare the energies obtained at different particle numbers. In [33], the authors found the energy, normalized by the noninteracting energy, to show only very weak dependence on the particle number when plotted against the rescaled

coupling,

$$\gamma = \frac{\pi g}{\sqrt{\omega N}}. \quad (\text{B1})$$

This behavior is reproduced by our data, as can be seen in Fig. 6(b), where we compare the energies against those of the two-particle system in the ground state. The lattice results generally overshoot the two-particle system slightly, which is expected at higher particle number, but may also partially result from the finite temperature.

Our current approach is somewhat limited in the couplings that can be studied, as stronger interactions lead to ergodicity issues in the Markov process. This makes tuning the particle number challenging, in particular at very low chemical potentials. Similar issues are encountered in the Hubbard model at half filling, where the issue can be mitigated by global updates [65]. Alternatively, it may be possible to circumvent the problem by sampling the canonical weight more directly.

APPENDIX C: APPROACH TO THE CONTINUUM

To demonstrate the proximity of our computations to the continuum theory, we compare the density profiles of the $N = 20$ balanced system with $g/\sqrt{\omega} = -3$ at various filling values. To this end, we keep the extent of the lattice fixed in units of the harmonic oscillator $N_x/L_T = 20$, while varying the number of lattice sites between $N_x = 24$ and 200 . Note that this procedure requires a retuning of the coupling for each lattice as described in Sec. III A. The results are shown in Fig. 7. We find the density profile around the center of the trap to be well converged, even for lattices with only 40 points. In contrast, smaller lattice sizes show clear signs of saturation. As can be seen in the inset, the $N_x = 80$ and 200 lattices show good agreement in the tails over eight orders of magnitude, after which they become indistinguishable from zero. We do not show the smaller lattices in the inset to avoid visual clutter.

-
- [1] G. Zürn, F. Serwane, T. Lompe, A. N. Wenz, M. G. Ries, J. E. Bohn, and S. Jochim, Fermionization of two distinguishable fermions, *Phys. Rev. Lett.* **108**, 075303 (2012).
- [2] T. E. Drake, E. Sagi, R. Paudel, J. T. Stewart, J. P. Gaebler, and D. S. Jin, Direct observation of the Fermi surface in an ultracold atomic gas, *Phys. Rev. A* **86**, 031601(R) (2012).
- [3] A. N. Wenz, G. Zürn, S. Murmann, I. Brouzos, T. Lompe, and S. Jochim, From few to many: Observing the formation of a Fermi sea one atom at a time, *Science* **342**, 457 (2013).
- [4] M. G. Ries, A. N. Wenz, G. Zürn, L. Bayha, I. Boettcher, D. Kedar, P. A. Murthy, M. Neidig, T. Lompe, and S. Jochim, Observation of pair condensation in the quasi-2D BEC-BCS crossover, *Phys. Rev. Lett.* **114**, 230401 (2015).
- [5] C. Chin, R. Grimm, P. Julienne, and E. Tiesinga, Feshbach resonances in ultracold gases, *Rev. Mod. Phys.* **82**, 1225 (2010).
- [6] A. L. Gaunt, T. F. Schmidutz, I. Gotlibovych, R. P. Smith, and Z. Hadzibabic, Bose-Einstein condensation of atoms in a uniform potential, *Phys. Rev. Lett.* **110**, 200406 (2013).
- [7] M. Holten, L. Bayha, K. Subramanian, S. Brandstetter, C. Heintze, P. Lunt, P. M. Preiss, and S. Jochim, Observation of Cooper pairs in a mesoscopic two-dimensional Fermi gas, *Nature (London)* **606**, 287 (2022).
- [8] H. Moritz, T. Stöferle, K. Günter, M. Köhl, and T. Esslinger, Confinement induced molecules in a 1D Fermi gas, *Phys. Rev. Lett.* **94**, 210401 (2005).
- [9] F. Serwane, G. Zürn, T. Lompe, T. B. Ottenstein, A. N. Wenz, and S. Jochim, Deterministic preparation of a tunable few-fermion system, *Science* **332**, 336 (2011).
- [10] L. Bayha, M. Holten, R. Klemm, K. Subramanian, J. Bjerlin, S. M. Reimann, G. M. Bruun, P. M. Preiss, and S. Jochim, Observing the emergence of a quantum phase transition shell by shell, *Nature (London)* **587**, 583 (2020).
- [11] O. Juillet, F. Gulminelli, and P. Chomaz, Exact pairing correlations for one-dimensionally trapped fermions with stochastic mean-field wave functions, *Phys. Rev. Lett.* **92**, 160401 (2004).
- [12] M. Casula, D. M. Ceperley, and E. J. Mueller, Quantum Monte Carlo study of one-dimensional trapped fermions with attractive contact interactions, *Phys. Rev. A* **78**, 033607 (2008).
- [13] C. N. Gilbreth and Y. Alhassid, Pair condensation in a finite trapped Fermi gas, *Phys. Rev. A* **88**, 063643 (2013).

- [14] T. Zielinski, B. Ross, and A. Gezerlis, Pairing in two-dimensional Fermi gases with a coordinate-space potential, *Phys. Rev. A* **101**, 033601 (2020).
- [15] A. Richie-Halford, J. E. Drut, and A. Bulgac, Emergence of a pseudogap in the BCS-BEC crossover, *Phys. Rev. Lett.* **125**, 060403 (2020).
- [16] M. Holten, L. Bayha, A. C. Klein, P. A. Murthy, P. M. Preiss, and S. Jochim, Anomalous breaking of scale invariance in a two-dimensional Fermi gas, *Phys. Rev. Lett.* **121**, 120401 (2018).
- [17] M. J. H. Ku, A. T. Sommer, L. W. Cheuk, and M. W. Zwierlein, Revealing the superfluid lambda transition in the universal thermodynamics of a unitary Fermi gas, *Science* **335**, 563 (2012).
- [18] P. Fulde and R. A. Ferrell, Superconductivity in a strong spin-exchange field, *Phys. Rev.* **135**, A550 (1964).
- [19] A. I. Larkin and Y. N. Ovchinnikov, Nonuniform state of superconductors, *Zh. Eksp. Teor. Fiz.* **47**, 1136 (1964).
- [20] J. Carlson, S. Gandolfi, K. E. Schmidt, and S. Zhang, Auxiliary-field quantum Monte Carlo method for strongly paired fermions, *Phys. Rev. A* **84**, 061602(R) (2011).
- [21] H. Shi, S. Chiesa, and S. Zhang, Ground-state properties of strongly interacting Fermi gases in two dimensions, *Phys. Rev. A* **92**, 033603 (2015).
- [22] E. R. Anderson and J. E. Drut, Pressure, compressibility, and contact of the two-dimensional attractive Fermi gas, *Phys. Rev. Lett.* **115**, 115301 (2015).
- [23] A. Bulgac, J. E. Drut, and P. Magierski, Quantum Monte Carlo simulations of the BCS-BEC crossover at finite temperature, *Phys. Rev. A* **78**, 023625 (2008).
- [24] R. Rossi, T. Ohgoe, E. Kozik, N. Prokof'ev, B. Svistunov, K. Van Houcke, and F. Werner, Contact and momentum distribution of the unitary Fermi gas, *Phys. Rev. Lett.* **121**, 130406 (2018).
- [25] Y.-Y. He, H. Shi, and S. Zhang, Precision many-body study of the Berezinskii-Kosterlitz-Thouless transition and temperature-dependent properties in the two-dimensional Fermi gas, *Phys. Rev. Lett.* **129**, 076403 (2022).
- [26] S. Ramachandran, S. Jensen, and Y. Alhassid, Pseudogap effects in the strongly correlated regime of the two-dimensional Fermi gas, [arXiv:2212.14880](https://arxiv.org/abs/2212.14880).
- [27] T. Sowiński, T. Grass, O. Dutta, and M. Lewenstein, Few interacting fermions in a one-dimensional harmonic trap, *Phys. Rev. A* **88**, 033607 (2013).
- [28] P. D'Amico and M. Rontani, Pairing of a few Fermi atoms in one dimension, *Phys. Rev. A* **91**, 043610 (2015).
- [29] L. Rammelmüller, D. Huber, M. Čufar, J. Brand, H.-W. Hammer, and A. G. Volosniev, Magnetic impurity in a one-dimensional few-fermion system, *SciPost Phys.* **14**, 006 (2023).
- [30] L. Rammelmüller, D. Huber, and A. G. Volosniev, A modular implementation of an effective interaction approach for harmonically trapped fermions in 1D, *SciPost Phys. Codebases* **12** (2023).
- [31] C. E. Berger, E. R. Anderson, and J. E. Drut, Energy, contact, and density profiles of one-dimensional fermions in a harmonic trap via nonuniform-lattice Monte Carlo calculations, *Phys. Rev. A* **91**, 053618 (2015).
- [32] C. E. Berger, J. E. Drut, and W. J. Porter, Hard-wall and non-uniform lattice Monte Carlo approaches to one-dimensional Fermi gases in a harmonic trap, *Comput. Phys. Commun.* **208**, 103 (2016).
- [33] T. Grining, M. Tomza, M. Lesiuk, M. Przybytek, M. Musiał, R. Moszynski, M. Lewenstein, and P. Massignan, Crossover between few and many fermions in a harmonic trap, *Phys. Rev. A* **92**, 061601(R) (2015).
- [34] T. Grining, M. Tomza, M. Lesiuk, M. Przybytek, M. Musiał, P. Massignan, M. Lewenstein, and R. Moszynski, Many interacting fermions in a one-dimensional harmonic trap: a quantum-chemical treatment, *New J. Phys.* **17**, 115001 (2015).
- [35] D. Pęcał and T. Sowiński, Unconventional pairing in few-fermion systems at finite temperature, *Sci. Rep.* **12**, 17476 (2022).
- [36] M. J. Wolak, V. G. Rousseau, C. Miniatura, B. Grémaud, R. T. Scalettar, and G. G. Batrouni, Finite-temperature quantum Monte Carlo study of the one-dimensional polarized Fermi gas, *Phys. Rev. A* **82**, 013614 (2010).
- [37] L. Rammelmüller, J. E. Drut, and J. Braun, Pairing patterns in one-dimensional spin- and mass-imbalanced Fermi gases, *SciPost Phys.* **9**, 014 (2020).
- [38] L. Rammelmüller, Y. Hou, J. E. Drut, and J. Braun, Pairing and the spin susceptibility of the polarized unitary Fermi gas in the normal phase, *Phys. Rev. A* **103**, 043330 (2021).
- [39] F. Attanasio, L. Rammelmüller, J. E. Drut, and J. Braun, Pairing patterns in polarized unitary Fermi gases above the superfluid transition, *Phys. Rev. A* **105**, 063317 (2022).
- [40] H. Tajima, S. Tsutsui, and T. M. Doi, Low-dimensional fluctuations and pseudogap in Gaudin-Yang Fermi gases, *Phys. Rev. Res.* **2**, 033441 (2020).
- [41] Y.-Y. He, H. Shi, and S. Zhang, Reaching the continuum limit in finite-temperature *ab initio* field-theory computations in many-fermion systems, *Phys. Rev. Lett.* **123**, 136402 (2019).
- [42] T. Busch, B.-G. Englert, K. Rzazewski, and M. Wilkens, Two cold atoms in a harmonic trap, *Found. Phys.* **28**, 549 (1998).
- [43] R. Blankenbecler, D. J. Scalapino, and R. L. Sugar, Monte Carlo calculations of coupled boson-fermion systems. I, *Phys. Rev. D* **24**, 2278 (1981).
- [44] D. J. Scalapino and R. L. Sugar, Monte Carlo calculations of coupled boson-fermion systems. II, *Phys. Rev. B* **24**, 4295 (1981).
- [45] J. E. Hirsch, Discrete Hubbard-Stratonovich transformation for fermion lattice models, *Phys. Rev. B* **28**, 4059 (1983).
- [46] S. R. White, D. J. Scalapino, R. L. Sugar, E. Y. Loh, J. E. Gubernatis, and R. T. Scalettar, Numerical study of the two-dimensional Hubbard model, *Phys. Rev. B* **40**, 506 (1989).
- [47] C. Bauer, Fast and stable determinant quantum Monte Carlo, *SciPost Phys. Core* **2**, 011 (2020).
- [48] W. E. Ormand, D. J. Dean, C. W. Johnson, G. H. Lang, and S. E. Koonin, Demonstration of the auxiliary-field Monte Carlo approach for *sd*-shell nuclei, *Phys. Rev. C* **49**, 1422 (1994).
- [49] C. Gilbreth, S. Jensen, and Y. Alhassid, Reducing the complexity of finite-temperature auxiliary-field quantum Monte Carlo, *Comput. Phys. Commun.* **264**, 107952 (2021).
- [50] S. Zhang, Auxiliary-field quantum Monte Carlo for correlated electron systems, in *Emergent Phenomena in Correlated Matter*, Schriften des Forschungszentrums Jülich Reihe Modeling and Simulation, Vol. 3, edited by E. Pavarini, E. Koch, and U. Schollwöck (Forschungszentrum Jülich, Jülich, 2013), pp. 15.1–15.28.

- [51] P. D'Amico and M. Rontani, Three interacting atoms in a one-dimensional trap: a benchmark system for computational approaches, *J. Phys. B: At. Mol. Opt. Phys.* **47**, 065303 (2014).
- [52] G. Zürn, A. N. Wenz, S. Murmann, A. Bergschneider, T. Lompe, and S. Jochim, Pairing in few-fermion systems with attractive interactions, *Phys. Rev. Lett.* **111**, 175302 (2013).
- [53] T. Duguet, P. Bonche, P.-H. Heenen, and J. Meyer, Pairing correlations. II. Microscopic analysis of odd-even mass staggering in nuclei, *Phys. Rev. C* **65**, 014311 (2001).
- [54] O. Goulko and M. Wingate, Thermodynamics of balanced and slightly spin-imbalanced Fermi gases at unitarity, *Phys. Rev. A* **82**, 053621 (2010).
- [55] M. J. Wolak, B. Grémaud, R. T. Scalettar, and G. G. Batrouni, Pairing in a two-dimensional Fermi gas with population imbalance, *Phys. Rev. A* **86**, 023630 (2012).
- [56] F. Attanasio, M. Bauer, and J. M. Pawłowski, Density profiles and correlations of harmonically trapped ultracold fermions via complex Langevin, *PoS* **430**, 363 (2023).
- [57] A. Alexandru, P. F. Bedaque, and N. C. Warrington, Spin polarized nonrelativistic fermions in $1 + 1$ dimensions, *Phys. Rev. D* **98**, 054514 (2018).
- [58] T. M. Doi, H. Tajima, and S. Tsutsui, Complex Langevin study for polarons in a one-dimensional two-component Fermi gas with attractive contact interactions, *Phys. Rev. Res.* **3**, 033180 (2021).
- [59] J. Dobrzyniecki, G. Orso, and T. Sowiński, Unconventional pairing in few-fermion systems tuned by external confinement, *Phys. Rev. Res.* **3**, 043105 (2021).
- [60] C. R. Shill and J. E. Drut, Virial coefficients of one-dimensional and two-dimensional Fermi gases by stochastic methods and a semiclassical lattice approximation, *Phys. Rev. A* **98**, 053615 (2018).
- [61] A. C. Loheac and J. E. Drut, Third-order perturbative lattice and complex Langevin analyses of the finite-temperature equation of state of nonrelativistic fermions in one dimension, *Phys. Rev. D* **95**, 094502 (2017).
- [62] F. Attanasio and J. E. Drut, Thermodynamics of spin-orbit-coupled bosons in two dimensions from the complex Langevin method, *Phys. Rev. A* **101**, 033617 (2020).
- [63] P. Heinen and T. Gasenzer, Complex Langevin approach to interacting Bose gases, *Phys. Rev. A* **106**, 063308 (2022).
- [64] P. Heinen and T. Gasenzer, Simulating the Berezinskii-Kosterlitz-Thouless transition with the complex Langevin algorithm, *Phys. Rev. A* **108**, 053311 (2023).
- [65] R. T. Scalettar, R. M. Noack, and R. R. P. Singh, Ergodicity at large couplings with the determinant Monte Carlo algorithm, *Phys. Rev. B* **44**, 10502 (1991).